Effect of High Pressure on Internally Self-Assembled Lipid Nanoparticles: A Synchrotron Small Angle X-ray Scattering (SAXS) Study

Chandrashekhar V. Kulkarni[a,b]*, Anan Yaghmur[c], Milos Steinhart[d†], Manfred Kriechbaum[e] and Michael Rappolt[e,f]

[a] *Biological and Soft Systems, Cavendish Laboratory, University of Cambridge, JJ Thomson Avenue, Cambridge CB3 0HE, United Kingdom*

[b] *Centre for Materials Science, School of Physical Sciences and Computing, University of Central Lancashire, Preston PR1 2HE, United Kingdom*

[c] *Department of Pharmacy, Faculty of Health and Medical Sciences, University of Copenhagen, DK-2100 Copenhagen, Denmark*

[d] *Institute of Macromolecular Chemistry, Academy of Sciences of the Czech Republic, Prague, Czech Republic*

[e] *Institute of Inorganic Chemistry, Graz University of Technology, A-8010 Graz, Austria.*

[f] *School of Food Science & Nutrition, University of Leeds, Leeds LS2 9JT, UK*

[†] *Present Address: Institute for Applied Physics and Mathematics, University of Pardubice, Studentska 84, 532 10 Pardubice, Czech Republic*

*Corresponding author email: cvkulkarni@uclan.ac.uk, Tel: +44-1772-89-4339, Fax: +44-1772-89-4981

KEYWORDS: Internally self-assembled lipid nanoparticles, cubosomes, hexosomes, lipid self-assembly, hydrostatic pressure, high pressure stability

ABSTRACT

We present the first report on the effect of hydrostatic pressure on colloidally stabilized lipid nanoparticles enveloping inverse non-lamellar self-assemblies in their interiors. These internal self-assemblies were systematically tuned into bicontinuous cubic (*Pn3m* and *Im3m*), micellar cubic (*Fd3m*), hexagonal (H_2), and inverse micellar (L_2) phases by regulating the lipid-oil ratio while the hydrostatic pressure was varied from atmospheric pressure to 1200 bar, and back to the atmospheric pressure. The pressure effect on these lipid nanoparticles was compared with their equilibrium bulk, non-dispersed counterparts, i.e. inverse non-lamellar liquid crystalline phases and micellar solutions under excess water conditions using synchrotron small angle X-ray scattering (SAXS) technique. In the applied pressure-range, induced phase transitions were solely observed in fully hydrated bulk samples; whereas the internal self-assemblies of the corresponding lipid nanoparticles displayed only pressure-modulated single phases. Interestingly both, the lattice parameters and linear pressure expansion coefficients were larger for the self-assemblies enveloped inside the lipid nanoparticles as compared to the bulk states. This can in part be attributed to enhanced lipid layer undulations in the lipid particles in addition to induced swelling effects in presence of the tri-block copolymer F127. The bicontinuous cubic phases in both bulk state and inside lipid cubosome nanoparticles swell on compression, even so both keep swelling further on decompression at relatively high pressures before shrinking again at ambient pressures. Pressure dependence of the phases is also modulated by the concentration of the solubilized oil (tetradecane). These studies demonstrate the tolerance of lipid nanoparticles (cubosomes, hexosomes, micellar cubosomes, and emulsified microemulsions (EMEs)) for high pressures proving their robustness for various technological applications.

1. INTRODUCTION

Biogenic lipids have a general tendency to self-assemble into lamellar liquid crystalline phases and/or inverse (*type 2*) lyotropic non-lamellar phases when mixed with water[1-3]. Lamellar (fluid- L_α, gel- L_β or crystalline- L_c) phases, an inverse micellar solution (L_2), and an inverse hexagonal (H_2) phase are commonly observed, however some lipids also form inverse bicontinuous cubic phases at ambient temperatures[3]. The latter exhibit geometrical basis of mathematically minimal surfaces of primitive (*P*), diamond (*D*) and gyroid (*G*) types with the corresponding space groups *Im3m*, *Pn3m* and *Ia3d*[4-6]. Upon addition of polar and non-polar components to certain binary lipid-water mixtures, it is possible to induce the formation of other phases including micellar (discontinuous) cubic *Fd3m* and sponge (L_3) phases[4-5, 7].

The lyotropic non-lamellar liquid crystalline phases have been exploited in various applications including crystallization of membrane proteins[8-9], solubilization of biomolecules[10-11], development of drug delivery matrices with sustained drug release properties[12], and separation of biomolecules[13]. For some of these applications, however, the non-lamellar phases need to be dispersed due to some evident reasons. For instance, the bicontinuous cubic phases are not easy to manipulate owing to their excessive viscosity[14]. Moreover, precise harvesting and delivery of same quantities of bulk phases each time is highly difficult due to their non-fluid (viscoelastic) character[15]. Therefore, it is advantageous to fragment these bulk phases into nanoparticles exhibiting a size in the order of a few hundreds of nanometers by applying an external high-energy input. This is commonly achieved by means of ultra-sonication or micro-fluidization in presence of efficient stabilizers[16-17]. Resulting nanostructured emulsions are similar to normal oil-in-water (O/W) emulsions, where the oil phase mainly consists of a lipid (or a lipid mixture) with propensity to form inverse non-lamellar liquid crystalline phases[17]. These discrete lipid nanoparticles have unique features as they envelop self-assemblies[17] inside their cores while imparting water-like fluidity to the aqueous dispersion. Based on the type of self-assembly, the dispersions are named as cubosomes for particles enveloping inverse bicontinuous cubic phases, hexosomes for particles enveloping inverse hexagonal (H_2) phase, etc.[4, 18] These nanostructured O/W emulsions are also recognized with the general term - *isasomes* - meaning *internally self-assembled particles* (note, "*soma*" is the Greek word for "*body*")[19].

The development of liquid crystalline nano-particulate formulations with low viscosity is desirable for their use in various pharmaceutical and food applications[5, 20].

Nanostructured lipid particles enveloping inverse *non-lamellar* liquid crystalline phases differ largely in their features from the most investigated lamellar lipid dispersions, i.e. vesicles. For instance, they exhibit a much larger surface area to particle volume ratio[21]. Moreover, vesicles are formed of one (uni-lamellar), a few (oligo-lamellar) or more (multi-lamellar) lipid bilayers enclosing water in their 'hydrophilic' cores, while *particles enveloping inverse non-lamellar liquid crystalline or micellar phase* consist *mainly* of 'hydrophobic' interiors (with a little hydrophilic regions) fabricated from the self-assembled nanostructure of one or more of the following types: bicontinuous cubic (*Pn3m*, *Im3m*), micellar cubic (*Fd3m*), hexagonal (H_2), inverse micelles (L_2), and sponge (L_3)[4]. It is interesting to note that similar particles, with hydrophobic cores, are also observed in biological entities, and are known as lipid droplets, lipid particles, oily bodies, oleosomes, or spherosomes[22-23]. Among these nano-objects, the lipid droplets are dissimilar structures to the cellular membranes and play a major role in metabolic functions[22]. Their most common function is the storage of lipids as an energy source[22]. They also supply components required for membrane biogenesis[22]. These lipid droplets are structurally related to other membranous organelles; a very good example is the evolution of the membrane of lipid droplets from the endoplasmic reticulum (ER) and the reported evidence of characteristic continuity among them[22]. Similar to biomembranes, these lipid droplets also undergo structural re-organization during their formation[22] and functioning[24-25]. In this context, nanostructured nanoparticles formed from simple lipid systems (as employed here) could work as appropriate model systems for gaining insight into some of the above mentioned structural and morphological changes. Moreover, these investigations are beneficial for the potential use of these nano-objects in a range of biotechnological applications, where the stability of the original phase and inter-transitions could play important roles, e.g. for drug delivery applications[26-28].

In this work, we investigate the pressure-dependent phase behaviour of nanostructured lipid particles and inverse bulk (non-dispersed) self-assemblies prepared in an aqueous medium using two different lipids, Dimodan U/J (DU, a commercial distilled unsaturated monoglyceride) and phytantriol (PT) together with varying amounts of the oil tetradecane (TC). The nanostructural characteristics of both dispersed and non-dispersed samples at different pressures in the range of 1-1200 bar at 25 ºC were tested in a compression-

decompression cycle by coupling pressure manipulations with synchrotron small angle X-ray scattering (SAXS) measurements. This pressure range (up to about 1000 bar) is considered crucial for biological functioning, above which many biomolecules start to denature or dissociate[29]. It should be noted that most of the earlier studies in literature were focused on the effect of pressure on equilibrium non-lamellar liquid crystalline, bulk phases. These studies involved, the effects of hydrostatic[30-33] and hydrodynamic[34-37] pressure on pure lipids and their mixtures under dry (solvent-free lipid), limited hydration, or excess water conditions. Most of these reports were focused on understanding isothermal pressure-induced structural alterations and dynamic phase transitions of the lipid crystalline and liquid crystalline phases[30-31, 38-42]. In advantage to temperature, pressure equilibrates homogenously and rapidly with the speed of sound within the sample and therefore it has triggered great interest in coupling rapid pressure induction experiments with synchrotron X-ray sources to capture the membrane dynamics and monitor in real time kinetics of phase transitions within microseconds[36]. This allowed tracking the transient intermediate phases in a more precise manner and led to an improved understanding of the topological membrane transformations [35, 37, 43]. The effect of pressure on the energetics and pivotal surface and its contribution in fine-tuning the dimensions of the lipid bicontinuous cubic phases were also reported recently[44,45]. Moreover, the pressure has been applied to investigate the interaction of various biomolecules[38, 44, 46-48] with lipid membranes, motivated by the development of biomimetic models of organisms (piezeophiles or barophiles) found under high pressure conditions of deep oceans[49]. Despite of these studies, there is no report, to the best of our knowledge, on the pressure-dependence of internally self-assembled nanostructures in cubosomes, hexosomes, and other related nanostructured emulsions as presented here.

2. EXPERIMENTAL METHODS

2.1 Materials

The used lipids: Dimodan U/J® (DU) was a generous gift from Danisco, Denmark, and phytantriol (PT) was kindly provided by Adina Cosmetic Ingredients, UK (local distributor of DSM Nutritional Products AG, Switzerland). DU is a commercial lipid containing distilled glycerides, of which 96% are monoglycerides while the rest are diglycerides and free fatty acids. Glycerol monolinoleate (62%) and glycerol monooleate (25%) constitute its main

monoglycerides. The hydrophobic part of DU is thus made up mainly of C_{18} chains (91%). The DU was chosen as a main lipid because its phase behaviour on exposure to water is very similar to that reported for the most investigated pure lipid glycerol monooleate, also known as monoolein (MO),[14, 50] and it has been extensively used for fabrication of various nanostructured lipid particles[17]. Pluronic© F127 was used as a stabilizer to stabilize nanostructured emulsions. It is a triblock copolymer made of polyethylene oxide and polypropylene oxide blocks (PEO_{99} -PPO_{67}-PEO_{99}). Tetradecane (TC) was used as an oil and its ratio with DU or PT was altered to control the type of lipid self-assembled nanostructure as shown in a previously reported phase diagram[51]. F127 and TC were purchased from Sigma-Aldrich, UK. All ingredients were stored in a fridge and used without further purification. The used water was purified using Barnstead Nanopure, Thermoscientific (USA).

2.2 Preparation of bulk non-dispersed lipid phases

Bulk non-dispersed phases were prepared using 1 g of a lipid (DU or PT) or a binary lipid mixture (lipid+oil) and equivalent weight of aqueous phase ensuring that the lipid phases are in excess water region according to the corresponding phase diagrams of DU and PT[14, 52]. Both lipids, usually form cubic *Pn3m* phase in excess water at ambient temperatures[14, 52], however, for current investigations we used 0.5 wt% aqueous solution of F127 instead of pure water. This aqueous concentration was chosen according to the studies by Salonen et al., who demonstrated the 'excess water boundary' for bulk phases (with oil) resides well below 50% water, and it decreases further with increasing oil content[53]. The molecular structure of the used lipids and the polymeric stabilizer F127 are presented in Fig. 1. The ratio between the lipid (DU or PT) and oil (TC) was controlled by δ value, which is defined by equation (1) [54].

$$\delta = \frac{m_{lipid}}{m_{lipid}+m_{oil}} \times 100 \qquad (1)$$

where, m_{lipid} and m_{oil} are masses of lipid (DU or PT) and solubilized oil (TC), respectively.

The lipid compositions (i.e. δ values) were chosen carefully to obtain a range of different phases[51] as shown in Fig. 1b (note that δ = 100 means oil-free sample: 100% lipid and 0% oil).

After mixing the components (a lipid or a lipid+oil binary mixture and F127 solution) in an Eppendorf tube, the samples were subjected to twenty freeze-thaw cycles with an intermittent mixing by a needle spatula. The needle spatula was prepared *in-house* by cutting a sharp part of the dispensing syringe needle and flattening the rest of the tip. This spatula is small enough to reach the bottom of an Eppendorf tube for an efficient mixing, especially, of viscous lipid liquid crystalline phases. These samples were then allowed to stand at room temperature for at least 24 h prior to the pressure studies.

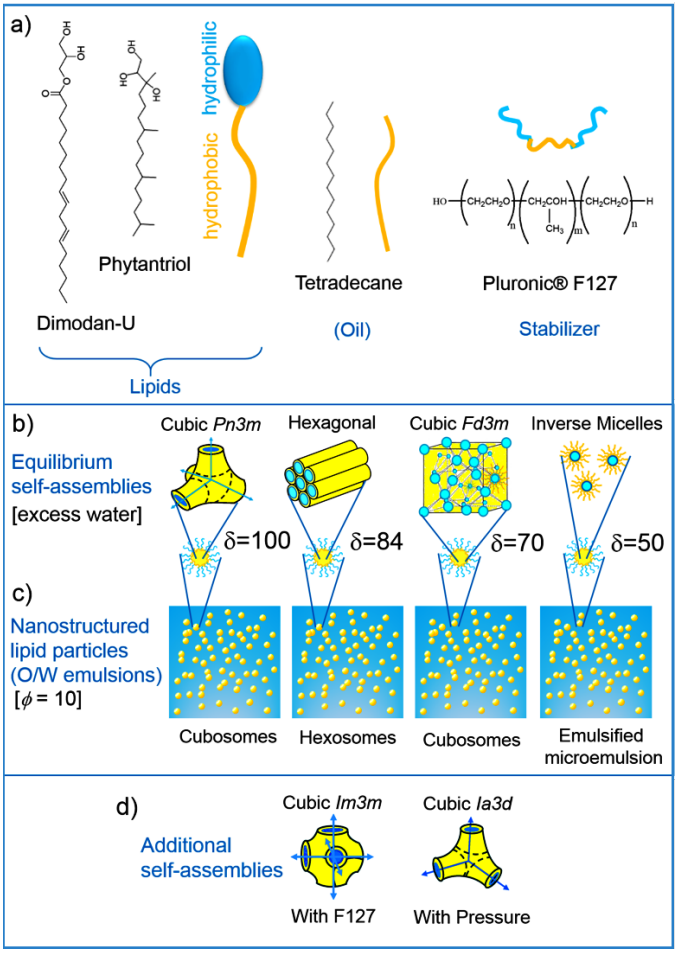

Fig. 1 Lipid composition and types of lipid self-assemblies: a) Chemical structures of lipids (DU and PT), an oil (TC), and a stabilizer F127. Blue and yellow colours, respectively, are codes for hydrophilic and hydrophobic moieties of the amphiphilic molecules (not in scale), which are supposed to aid in understanding the self-assembly process and the emulsion steric stabilization mechanism. b) By tuning the δ value, i.e. the composition of the lipid phase, the type of self-assembly can be controlled as shown by illustrations for inverse non-dispersed (equilibrium) bulk liquid crystalline phases and inverse micellar phase in their equilibrium states. c) Self-assembled nanostructures shown in b) were kinetically stabilized using the polymeric stabilizer F127 to form O/W emulsions (structured aqueous dispersions) comprised of lipid nanoparticles. d) Schematics for the inverse bicontinuous cubic *Im3m* and *Ia3d* phases; these phases were experimentally detected in the bulk states

of DU and PT due to the incorporation of F127 to the non-lamellar liquid crystalline phase and the application of high pressure, respectively.

2.3 Preparation of nanostructured lipid particles

In the present work, the nanostructured lipid particles were prepared using similar lipid phase compositions as above (equation (1))[54], but the proportion of the aqueous phase (aqueous medium containing 0.5% F127) was considerably higher than that used for preparing the fully hydrated bulk non-dispersed phases: the value of $\phi = 10$ as defined by equation (2) indicates the formation of nanostructured emulsions composed of 10 wt% 'dispersed phase' and 90 wt% aqueous medium.

$$\emptyset = \frac{m_{lipid}+m_{oil}}{m_{water}+m_{lipid}+m_{oil}} \times 100 \qquad (2)$$

where, m_{water} is the mass of water.

The lipids (DU or PT) and their binary mixtures with TC were subjected to ultra-sonication by using the Sonics Vibracell VCX 130 processor (Sonics & Materials Inc., Newton, Connecticut, USA) at 35% of the maximum power with 1 sec pulse time and 1 sec delay for a total time of 20 min. Fig. 1 shows schematics of the dispersions and corresponding types of internal self-assemblies. The size of lipid nanoparticles ranged typically from 250-480 nm as determined by dynamic light scattering technique (data not shown).

2.4 Synchrotron small angle X-ray scattering (SAXS)

SAXS measurements were performed at the Austrian SAXS beamline at the synchrotron radiation source Elettra (Sincrotrone Trieste, Italy); more details are published earlier[55]. A typical exposure time of 300 sec was used to obtain well-defined patterns of dispersed particles; only in a few cases of lower signal-to-noise ratio it was increased to 420 sec. For bulk phases, 120 sec exposure time was adequate. SAXS patterns obtained at the synchrotron source were analysed using AXcess software package (based on IDL Language) developed by 'Membrane Biophysics' research group at Imperial College London, UK. Two-dimensional (2-D) patterns were integrated into 1-D plots of intensity (arbitrary units) versus scattering vector (q in $Å^{-1}$) and calibrated with silver behenate having standard lattice spacing of 58.38 Å. The scattering vector q is defined as ($4\pi sin\theta/\lambda$), where 2θ = scattering angle and

λ = wavelength of radiation. Each phase displays a number of peaks positioned at characteristic ratios (Fig. 2). These ratios are well defined for each space group[5] (indicated in Fig. 2), and are used to calculate the lattice parameters of each self-assembled nanostructure. The lattice parameters were determined within an error of <1.0 Å.

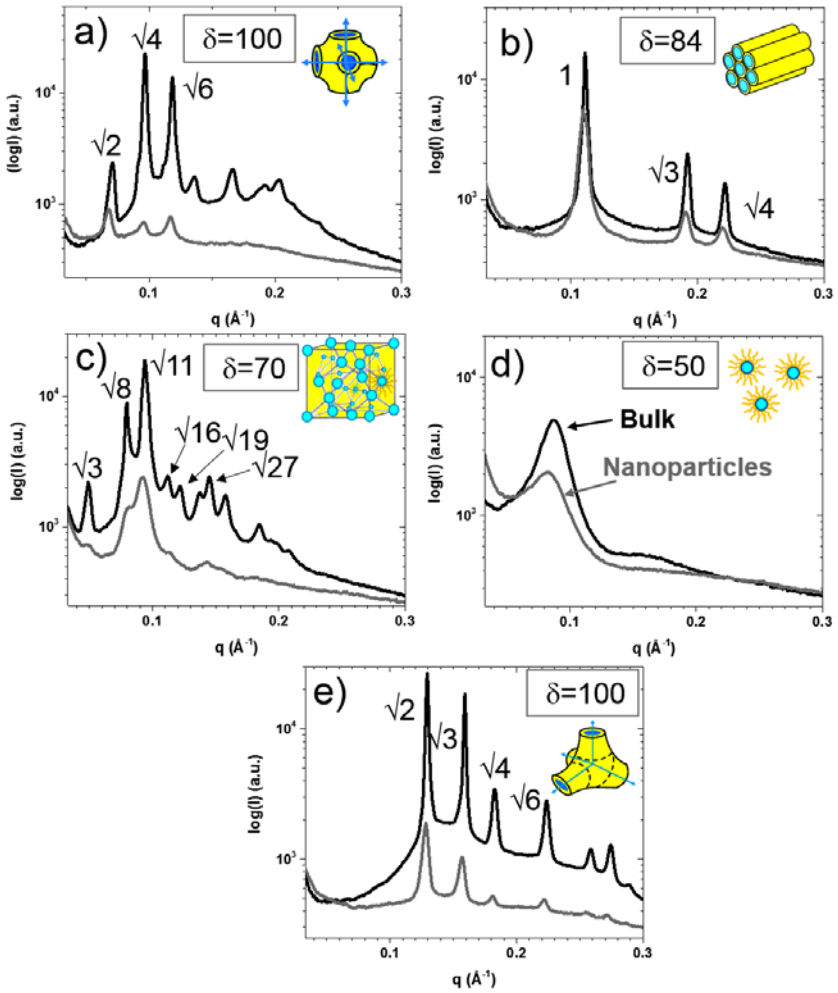

Fig. 2 SAXS patterns and identification of self-assemblies: Integrated plots of intensity *vs.* scattering vector (q) in 1-D are shown for bulk (black curves) and dispersed nanoparticles (grey curves) for DU (a) to d)) with varying δ values, and PT (e)) at ambient pressures and 25 °C. a) The inverse bicontinuous cubic *Im3m* phase, b) the inverse hexagonal (H_2) phase, c) the inverse micellar cubic *Fd3m* phase, d) the inverse micellar (L_2) phase were identified for samples exhibiting δ values of 100, 84, 70 and 50, respectively. In case of bulk DU (a)), the cubic *Im3m* co-existed with the cubic *Pn3m* phase (more evident from the contour plot in Figure 5d). e) PT shows neat cubic *Pn3m* phase for both bulk and dispersed samples. Corresponding Bragg reflections are designated for each phase, for instance, √2, √4, √6 for the cubic *Im3m* phase and so on.

2.5 Isothermal pressure scans

Pressure studies were performed using a high pressure X-ray cell; for details refer to relevant references[40, 56]. Briefly, the cell can produce pressures from atmospheric to 3500 bar using a remote controlled piston, which is connected *via* stainless steel tubing to a sample cell, wherein the sample gets commonly pressurized by water. The cell is sealed by two diamond windows with 0.5 mm thickness each and has an optical path length of 3.5 mm between the two windows. Closable capsules filled with 30 µl of lipid bulk non-dispersed samples or lipid particles were used in the current studies. All samples were subjected to upward pressure scan (compression scan) from 1 to 1200 bar with intermediate pressures of 100, 200, 400, 600, 800 and 1000 bar; whereas the downward scan (decompression scan) was done in the same steps omitting the 100 bar step. SAXS measurements were started after attaining static pressure conditions (usually waiting time of 2 min is required for obtaining a sufficient stationary pressure). These studies, in both compression-decompression scans, were performed at a constant temperature of 25±0.1 °C (thermostat: Unistat CC, Huber, Offenburg, Germany).

3. RESULTS

3.1 Pressure induced swelling of inverse hexagonal (H_2) and micellar cubic (*Fd3m*) phases

At δ value of 84, the DU/TC mixture in excess water tends to form H_2 phase at 25 °C and 1 bar; whereas it forms micellar cubic *Fd3m* phase at δ = 70[51]. The lattice parameter of the H_2 phase in the bulk state (at 1 bar) was found to be 56.6 Å, but the H_2 phase inside corresponding lipid particles was a little larger with a lattice parameter of 56.9 Å. Similarly, the lattice parameter for the bulk cubic *Fd3m* phase (226.3 Å) was smaller than the one inside lipid particles (227.1 Å). For bulk states, the H_2 phase swelled by 3.8 Å while the cubic *Fd3m* phase swelled by 15.2 Å at 1000 bar; see changes in lattice parameter (Δa) values in Table 1. These values were even higher for liquid crystalline phases inside the lipid particles (4.5 Å for the H_2 phase as compared to 16.0 Å for the cubic *Fd3m* phase) elucidating that the pressure has a stronger effect on the lipid particles than on the bulk states. Please note that our main focus is on discussing the structural alterations detected in the pressure interval between 1 to 1000 bar because all samples in this regime displayed a roughly linear dependence of the lattice parameters on pressure. The pressure-induced swelling of the H_2 and the cubic *Fd3m* phases compares well with previous studies by Yaghmur et al. on similar

(MO-TC) system[40]. Pressure increases the conformational order among hydrophobic chains thereby reducing the chain splay[36]. These molecular changes are accommodated through the enlargement of lattice parameters in presence of excess water[34, 38, 40, 57].

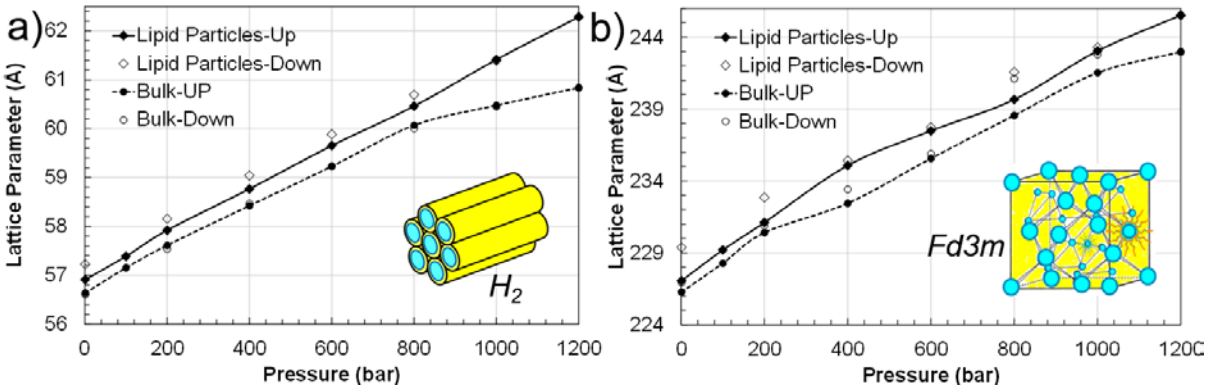

Fig. 3 Pressure effect on the H_2 (δ= 84) and the cubic *Fd3m* (δ= 70) phases: Lattice parameters of a) the H_2 and b) the cubic *Fd3m* phases with increasing (solid symbols) and decreasing (hollow symbols) pressures are reported. The lattice parameter values for mesophases inside the lipid particles are represented with diamonds, while the values for the bulk states are indicated by circles. Pressure-driven swelling of both phases can be clearly seen.

It was reported in previous studies that the isothermal changes in the lattice parameters of lyotropic liquid crystalline phases are usually monotonic with increasing pressure and follow a linear increase[40, 57]. However, a different behaviour could be detected when pressure variation is associated with significant structural alterations (occurrence of phase transitions and the evolvement of newly formed coexisting phases). During the upward pressure scan, the H_2 phase in the bulk state linearly swelled with the rate of 0.0042 Å·bar^{-1}, which lowered to 0.0018 Å·bar^{-1} after 800 bar. However, the H_2 phase inside the lipid particles swelled with a little higher rate (0.0044 Å·bar^{-1}). The rates for the cubic *Fd3m* phase were comparable (0.015 Å·bar^{-1}) for both bulk and particle states during upward pressure scans.

It was also interesting to examine the reversibility of the structural changes for both H_2 and *Fd3m* phases during the de-compression step. In the downward pressure scan (hollow symbols in Fig. 3), both phases closely followed the changes during upward pressure scans (solid symbols in Fig. 3) with a little hysteresis and the lattice parameters remained slightly higher, especially for the mesophases inside the lipid particles.

Table 1: Lipid compositions (shown by δ values), type of corresponding self-assembly, lattice parameters (*a* in Å) and swelling (Δ*a* in Å) with pressure (Δ*P* in bar) for bulk and dispersed nanoparticles are shown. NA: phase not available in the lipid nanoparticles or not detected at certain pressure in the bulk state. All SAXS experiments were performed at 25 °C.

Lipid	**δ values**	**Type of self-assembly**	**a (Å) bulk (1/1000 bar)**	**a (Å) particles (1/1000 bar)**	**Δa (Å) at ΔP =1000 bar for bulk**	**Δa (Å) at ΔP =1000 bar for particles**
DU	50	L_2*	73.2/77.2	76.4/81.4	4.0	5.0
DU	70	*Fd3m*	226.3/241.5	227.1/243.1	15.2	16
DU	84	H_2	56.6/60.4	56.9/61.4	3.8	4.5
DU	100	*Im3m*	127.7/133.6	132.1/138.8	5.9	6.7
DU	100	*Pn3m*	93.6/97.4	NA	3.8	NA
PT	100	*Pn3m*	68.4/72.2	69.4/79.5	3.8	10.1
PT	100	*Ia3d*	NA/114.1	NA	NA	NA

*The characteristic distance values are presented for the inverse micellar solution (L_2 phase).

3.2 Pressure effect on inverse micellar (L_2) phase

The inverse micellar (L_2) phase in the bulk state displayed a characteristic distance of 73.2 Å, which increased by 4.0 Å at 1000 bar, however, at 1200 bar the phase converted into a neat H_2 phase (Fig. 4). The lattice parameter of this H_2 phase (59.9 Å) was comparable with the lattice parameter of the H_2 phase (60.4 Å at 1000 bar) observed for the bulk phase that was prepared with a different composition (with δ value of 84 instead of 70) (Fig. 3). Upon decompression, i.e. during the downward pressure scan, the H_2 phase converted into cubic *Fd3m* phase at 1000 bar with a lattice parameter of 232.0 Å (see Fig. 4). With further decompression, however, the L_2 phase recovered back and its lattice spacing changed in the same manner as detected in the upward scan (Fig. 4). The above observed phase sequence is same as conventional phase transition (L_2-*cubic Fd3m*-H_2) in excess water based on average mean curvatures of phases[30].

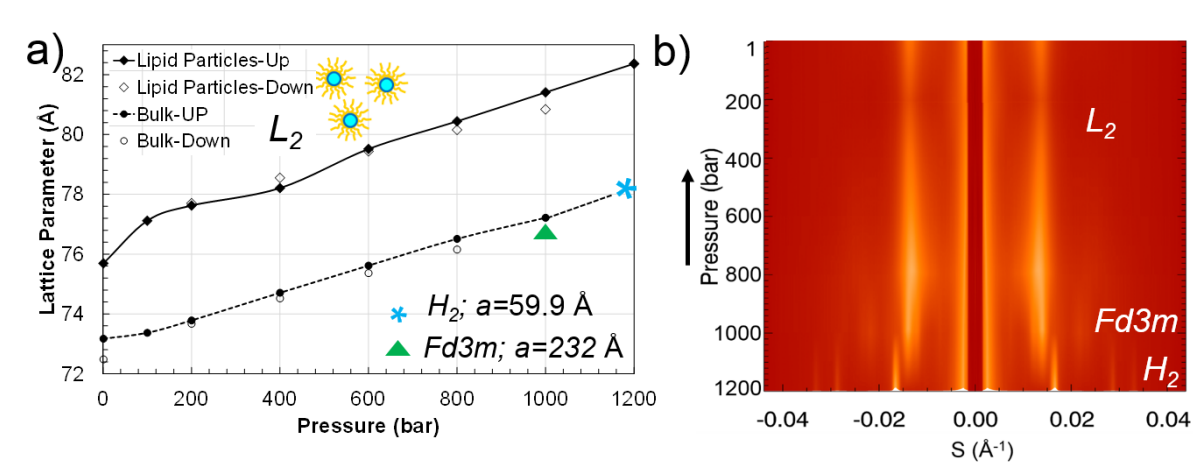

Fig. 4 Pressure effect mainly on the L_2 phase (δ= 50): a) Pressure effect on the L_2 phase in the bulk state (circles) and inside lipid particles (diamonds) for upward (solid symbols) and downward (hollow symbols) pressure scans. For the bulk sample, the phase transition from L_2 to H_2 (shown by an asterisk) was observed during the upward scan at 1200 bar, while an H_2 to cubic *Fd3m* phase (shown by a triangle) transition was recorded during the 'downward' scan at 1000 bar. The phase transitions are clearly detected as presented in the contour plot in panel b). The lattice parameters for the H_2 and the cubic *Fd3m* phases are not plotted in a), but the numbers are specified in the bottom legend.

No phase transitions were seen in case of the L_2 phase inside lipid particles (these dispersions are also known in literature as emulsified microemulsions, EMEs), but its characteristic nearest neighbour distance did increase when the sample was compressed (see Table 1). The rate of swelling for the L_2 phase inside lipid particles (0.0051 Å.bar^{-1}) was relatively larger than the rate for the bulk state (0.0042 Å.bar^{-1}) as determined in 400-1200 bar pressure range.

3.3 Coexistence and swelling behaviour of bicontinuous cubic phases

At δ = 100 (DU in excess water, no TC), DU is expected to show a bicontinuous cubic *Pn3m* phase[14], however, it is well known that some stabilizers like, e.g. F127, can induce a significant structural alteration in DU and also in other similar lipids[51, 58-59]. We observed a neat *Im3m* phase for DU particles, but a well pronounced co-existence of the cubic *Pn3m* and the cubic *Im3m* phases in case of bulk samples. Both phases were stable and persisted up to 1200 bar and also during the downward pressure scan. The characteristic Bonnet ratio for these coexisting cubic phases was in the range of 1.36-1.38 during upward scan while it was 1.33-1.39 during downward pressure scan. The Bonnet ratio values determined over the whole pressure range displayed a significant, but not uncommon deviation from the

theoretical value of 1.279[60], which most probably is related to non-equilibrium hydration conditions. The lattice parameter for the coexisting cubic *Pn3m* phase was found to be 93.6 Å at atmospheric pressure, which increased to 97.4 Å at 1000 bar; whereas the lattice parameter for the cubic *Im3m* increased from 127.7 to 133.6 Å. Such a swelling behaviour with pressure (from 132.1 to 138.8 Å) was also observed for the cubic *Im3m* phase inside lipid particles (Fig. 5).

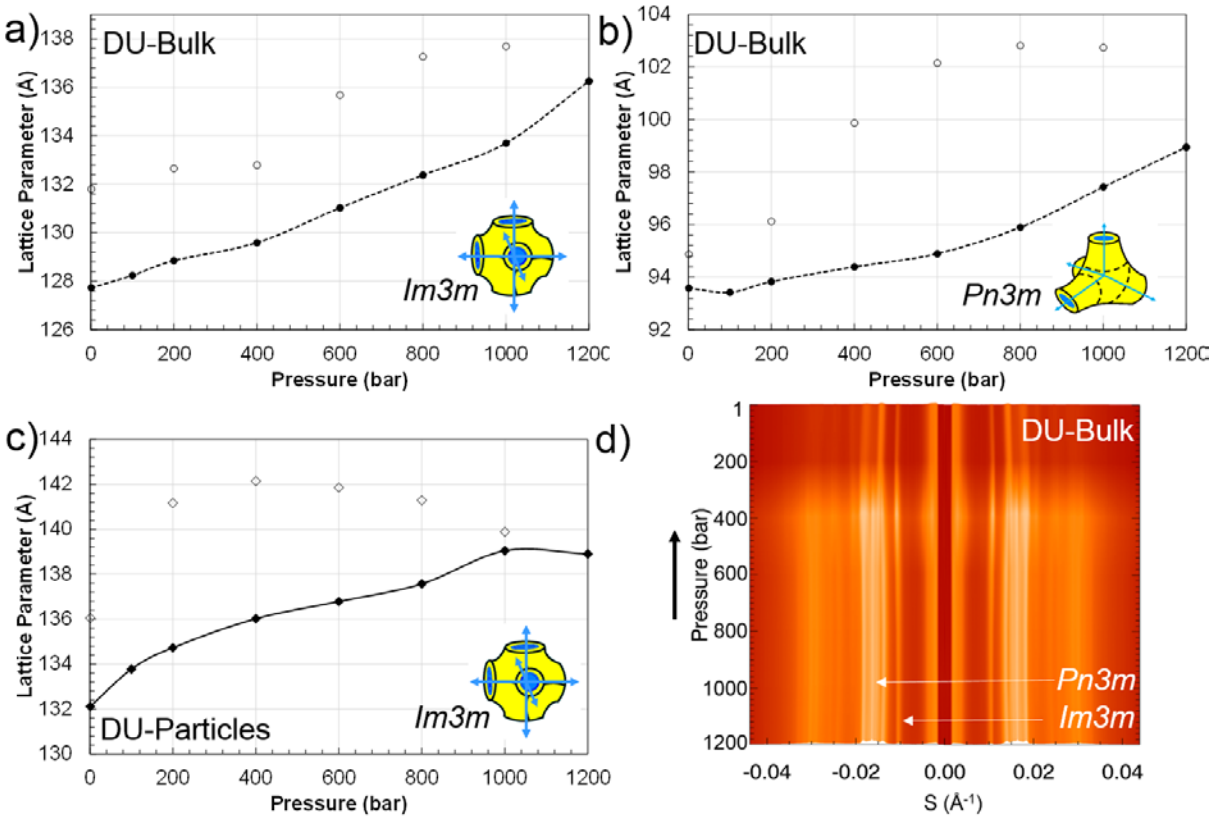

Fig. 5 Pressure effect and hysteresis of bicontinuous cubic phases (at δ= 100): Changes in the lattice parameters with pressure are shown for the coexisting phases a) the cubic *Im3m* and b) the cubic *Pn3m* for bulk DU sample, while changes in the sole cubic *Im3m* phase inside lipid particles are shown in c). Solid symbols represent upward and hollow symbol indicate downward pressure scans. d) The contour plot elucidates the coexistence of the cubic *Pn3m* and *Im3m* phases in the bulk sample during the 'downward' pressure scan. Pressure-triggered hysteresis can be clearly seen as the lattice parameters of the bicontinuous cubic phases do not follow the same paths during compression and decompression scans at 25 °C.

It is interesting to note that beforehand compressed phases kept swelling further during the decompression scan, and only after 800 bar they started shrinking again; the swelling was extended for the cubic *Im3m* phase inside lipid particles until 400 bar (Fig. 5). The cubic *Im3m* phase in bulk state swelled by 1.4 Å and the cubic *Pn3m* swelled by 3.9 Å during decompression from 1200 to 800 bar; whereas the cubic *Im3m* inside particles swelled by 3.2

Å. Strong hysteresis caused by application of pressure was evident for these phases as their lattice parameters followed completely different paths during upward and downward pressure scans. Occurrence of transient (swollen) phases and hysteresis are generally attributed to the dynamic processes including a complex interplay of water within the aqueous channels of the bicontinuous cubic phases and a delayed response of the lipid curved bilayers[37, 49]; however more work at different decompression rates is required to decouple and validate these mechanisms. Such effects are even more pronounced in pressure-jump experiments[35-37], demonstrating that the lattice parameters of the liquid crystalline phases in decompression scans are strongly scan rate dependent.

3.4 Pressure effect on PT-based bulk and dispersed samples: evolution of cubic *Ia3d* phase in the bulk state

Phytantriol (PT) exhibits cubic *Pn3m* phase in excess water at ambient temperatures and atmospheric pressure[52], which is generally retained in the presence of F127 molecules (Fig. 6)[61-62]. The lattice parameter of this phase in the bulk state was found to be 68.4 Å, while its value inside lipid particles was 69.4 Å. The lattice parameters were ~24 Å smaller than those detected for the cubic *Pn3m* phase in TC-free DU bulk sample (see Fig. 5). Initial rates of swelling for the cubic *Pn3m* phase were comparable (~0.009 Å·bar^{-1}) for both bulk and lipid particles based on PT, but the swelling of the bulk slowed down considerably after 200 bar (~0.003 Å·bar^{-1}). This could be attributed to the evolution of newly formed co-existing cubic *Ia3d* phase, which was detectable after 800 bar (Fig. 6) of compression. The degree of swelling for the cubic *Pn3m* phase in lipid particles was considerably higher than in the bulk state, with the lattice parameters differing by about 10.1 Å at 1000 bar.

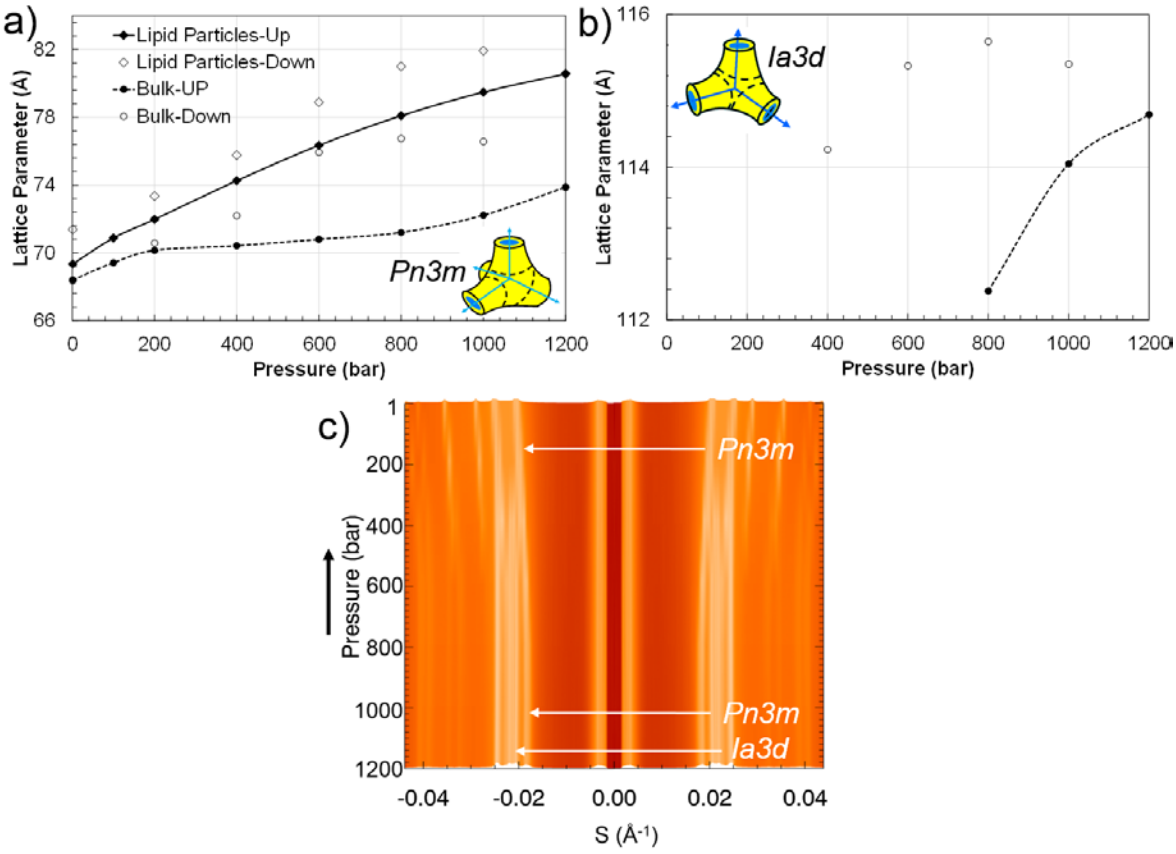

Fig. 6 Pressure effect on phytantriol (PT) bulk and dispersed systems (at δ = 100): Changes in the lattice parameters with pressure are shown for coexisting cubic phases a) the cubic *Pn3m* (circles) and b) the cubic *Ia3d* (circles) phases for bulk samples, while changes in the sole cubic *Pn3m* phase inside lipid particles are shown with diamond symbols in a). Solid symbols represent upward and hollow symbols indicate downward pressure scans. c) The contour plot elucidates the coexistence of cubic *Pn3m* and *Ia3d* phases in the range of 1200-400 bar for the bulk sample during the downward pressure scan.

During the downward scan, both the bulk cubic *Pn3m* and *Ia3d* phases showed a strong *hysteresis*, and thus, the lattice parameters for phases during the decompression step did not follow the trend of the upward pressure scan. Both phases swelled initially, followed by their shrinking with a further reduction in pressure (Fig. 6). The lowest lattice parameter for the cubic *Ia3d* phase was 112.3 Å at 800 bar during the compression scan, while the highest one was 115.6 Å in the decompression scan again at 800 bar. The lattice parameter for the monophasic cubic *Ia3d* phase at atmospheric pressure under limited hydration conditions was found to be 100.9 Å by Barauskas et al.[52] The characteristic Bonnet ratio for the pressure-induced coexistence of cubic *Ia3d* and *Pn3m* phases matched well with the theoretical value of 1.576[60] during upward pressure scan while a little deviation was seen during the downward pressure scan (1.50-1.58). It should be noted that the coexisting cubic *Ia3d* phase is not commonly seen in pure lipid systems at atmospheric pressure in excess water and for

hydrostatic pressure measurements performed under excess water conditions[34, 43]. Nevertheless, it was observed under limited water conditions at atomospheric pressure[33, 45] and when model lipids were mixed with biomolecules including membrane proteins,[46, 49, 63]and subjected to high hydrostatic pressures.

4. DISCUSSION

Bulk liquid crystalline state studies in the past were performed either under limited or excess water conditions[29-31, 33, 36, 38, 40, 45, 49]. The 'excess water boundary' (also called the maximum water solubilization line in phase diagrams) signifies that the inverse self-assembled nanostructure is not able to accommodate any further water[53, 64-65]. It is generally regarded as a 'biologically relevant' condition where physical properties, for instance, type of lipid phase, transition temperature, and lattice parameters remain constant with further addition of water[66]. Commonly, an excess water boundary for majority of unsaturated monoglycerides and PT is reported to be around water fraction of 0.4-0.5 (40-50 % water) or a bit lower at ambient temperatures and is sensitive to variations in lipid composition and the presence of guest additivies[14, 52-53, 65, 67-68]. In the current report, we used 50% aqueous solution of 0.5% F127 (by weight) to prepare the bulk samples and, therefore, the SAXS experiments were performed well above the excess water boundary for both DU-TC[53] and PT systems. The aqueous phase content for dispersed lipid particles was 90 wt% (ϕ = 10). Hence, the initial lattice parameters for all phases in both bulk and dispersed samples (1 bar) are expected to be identical under the assumption that the presence of stabilizer does not affect the structural features in both states. In other words, the stabilizer does not penetrate into the lipidic phases to modify their structural properties. We did not observe such behaviour as the lattice parameters of the self-assemblies in the bulk state were always lower than those determined for the phases inside lipid particles. Moreover, the cubic *Pn3m* phase in bulk DU sample coexisted with the *Im3m* phase (Fig. 5), and the latter was induced most likely by the stabilizer F127. In this respect, largely hydrophilic surfactant stabilizers, similar to F127, are anticipated to expand the hydrophilic headgroup area of the lipid molecules at the lipid-water interface thereby straightening their molecular shapes (from inverse cone towards cylindrical shape). Thus, they change the magnitude of the interfacial spontaneous curvature and induce significant structural alterations in the inverse non-lamellar liquid crystalline phases[59, 69-70]. The curvature change is compensated by an enlargement of the inverse self-assemblies and is

associated with structural transformations in F127 concentration dependent manner to phases with a lower interfacial curvature modulus, for instance as given in the F127-induced cubic *Pn3m* to *Im3m* transition[71]. Moreover, F127 may tend to be localized in the hydrophilic aqueous channels of the bicontinuous cubic phases and swell them transiently[70]. In the present work, the pressure effects are more pronounced in lipid particles because they have a higher relative proportion of F127 than the bulk state samples.

Another noteworthy fact is that the isothermal compressibility of the aqueous medium is lower than that of the lipidic media. Almost all of the lipid inverse self-assemblies in the bulk state consist of a denser lipidic medium – with isothermal compressibilities of about 165 x 10^{-6} bar^{-1}; [72] whereas, an aqueous continuous medium with the compressibility of 46 x 10^{-6} bar^{-1},[73] surrounds the self-assemblies within lipid particles. Moreover, the viscosity of lipid bulk phases is much greater than the surrounding aqueous medium, contributing further to the above mentioned isothermal compressibility values. It could also affect the diffusion of F127 from the surrounding continuous aqueous medium to the inverse self-assemblies on compressing/de-compressing the samples at 25 °C. In particular, for the bicontinuous cubic phases, the difference in compressibility is envisaged to affect the curved bilayer undulations where the lipid medium dampens them more than the aqueous medium. In the discontinuous phases (the L_2, the cubic *Fd3m*, and the H_2 self-assemblies), it concerns the undulations of the inverse micelles, where again it can be expected that dense lipidic medium (bulk state) dampens undulations to a greater extend as compared to the nano-particulate form. We note that earlier reports revealed that bilayer undulations are suppressed in the systems adsorbed on solid supports, which partly contribute to a reduction in lattice parameters[74]. The excess water boundary for unsupported/free-standing systems shifts towards higher hydration levels upon elevation in bilayer undulations[66]. To summarize, the self-assemblies inside lipid particles should encounter greater undulations of their building blocks (micelles and bilayers) due to the surrounding, less viscous aqueous medium, as compared to the bulk states. Last, another argument connected to a possible enhancement of undulations and overall bigger lattice spacings concerns the confined space given in particles that predictably could lead to a higher volume-fraction of defects. Principally, this is supported by the diffraction patterns of the bulk and nanoparticle samples, respectively (Fig. 2), where the latter display diffraction peaks with relatively broader central widths (FWHM) and a wider tailing off region (best seen in panels b, c and e). We note, that according to the Scherrer equation[75] the central width is mainly influenced by the average number of repeat units, *N*, being in diffraction condition

(FWHM $\propto 1/N$), while the peak shape and tailing off behaviour is governed by the type of disorder[76]. Unfortunately, defects would contribute to both, the peak width and shape, and it is nearly impossible to disentangle all three possible sources influencing peak broadening, i.e. crystallite size, pure undulation effects and volume fraction of defects. Advanced freeze fracture electron microscopy techniques might be helpful to solve this particular issue, but it is clearly going beyond the scope of the present study.

In conclusion, the aforementioned effects of isothermal compressibility and bilayer/monolayer undulations in combination with the possible insertion of F127 to the hydrophilic domains of the inverse non-lamellar self-assemblies may result into an elevation in excess water boundary thereby accommodating more solubilized water in both dispersed and non-dispersed bulk states. This view is supported by the noticeably larger lattice parameters of self-assemblies within lipid particles. With increasing pressure, self-assemblies in bulk state swell as expected,[34, 36, 41] but the ones inside lipid particles swell even more (Table 1).

It was reported that the complex interplay of water across the bilayer network in lamellar and inverse bicontinuous cubic liquid crystalline phases also plays a critical role during pressure scans and jumps[34, 36-37, 41]. It was proposed that intermediates or short-lived phases, frequently reported in such cases, act as reservoirs for accommodating excess water before the final stable phases are formed[34, 36-37, 41, 77-78]. Accordingly, we found that the cubic phases keep swelling further upon decompression (Fig. 5, 6) before they start shrinking again. The lattice parameters for phases during downward pressure scans appear to be considerably larger than those during upward pressure scans, at the same applied pressures. Interestingly, this was also detected for cubic phases inside the lipid cubosome particles. It is important to note that this swelling was strongest seen during decompression steps (and also in pressure-jump experiments)[37, 77] which may be deciphered to the slower reaction of compressed lipid structures on release of applied pressure. We note that the equilibration time (2 min) applied in our study is sufficient to guarantee enough time for water diffusion processes to be completed at least for the dispersed systems. It is known from T-jump experiments that the equilibration of water concentrations during lipid phase transitions in multilamellar liposomes are reached within few seconds[79], and hence the rearrangement of lipidic material in the bicontinuous phases in particular with respect to cubosomes is expected to be the true bottleneck. A possible explanation could lie in the fact that in compression direction the

number of unit cells diminishes (note, the total lipid volume remains nearly constant, while the unit-cell lipid volume increases significantly). Accordingly, in decompression direction the number unit cells increases, which might explain the slowed down decrease of the lattice parameter. In lay terms: it always takes longer to rebuild a house by putting bricks into place, than to destroy one. For phytantriol, we observed that the cubic *Ia3d* phase coexisting with *Pn3m* phase during the decompression scan (Fig. 6). The appearance of the cubic *Ia3d* during pressure scan has been reported for protein-lipid[46] and membrane protein-lipid system[49]. It is presumed that being a long molecule, similar to proteins, F127 could have comparable effects leading to the stabilization of the cubic *Ia3d* phase in the studied PT system.

Some self-assemblies studied here include oil (TC) as an additional component, which essentially interacts with the hydrophobic chains of the investigated amphiphilic lipids, DU and PT[40]. The water solubilisation capacity of mesophases is reported to decrease with an increase in oil content[19, 53]. This also is reflected in the systems subjected to high pressures. The isothermal compressibility (β_T) of TC is very low (0.91807×10^{-6} bar^{-1})[80] as compared to lipids (β_L =165×10^{-6} bar^{-1})[72]. Therefore in pressurised systems, the swelling is expected to decrease with increasing oil content. Fig. 7 demonstrates that the linear pressure expansion coefficient, $\Delta a/(a\,\Delta P)$, determined in the range from 1 to 1000 bar (for normalisation the mean lattice parameter, a, was considered in this range, i.e. $(a_{1\ bar}+a_{1000\ bar})/2$). Two important trends can be seen: (i) all dispersed systems display higher linear expansion rates, and (ii) in case of compressing discontinuous phases (L_2, *Fd3m* and H_2), the expansion coefficients do indeed drop with increasing oil content.

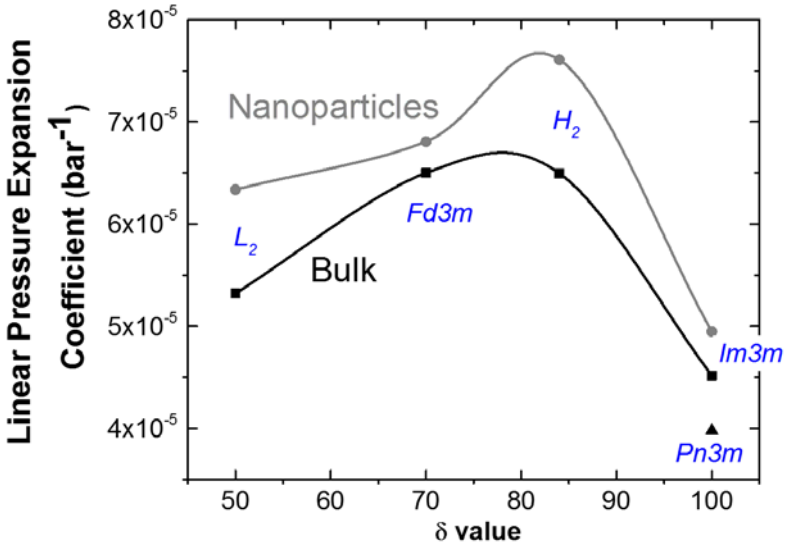

Fig. 7 Contribution of solubilized TC (oil) to the pressure-induced swelling of self-assembled nanostructures of DU: Changes in the linear pressure expansion coefficient ($\Delta a/(\Delta P\ a)$) as a function of solubilized oil (TC) content in the non-dispersed bulk and dispersed phases (in terms of δ value). The grey curve displays the behaviour for lipid particles, while the black curve refers to bulk samples. Among the discontinuous phases, the H_2 phase displays the highest expansion coefficient. The upward pressure scans for both lipid particles and the bulk state samples were used to generate these plots.

5. CONCLUSIONS AND PERSPECTIVES

Pressure effects on internally self-assembled lipid particles are presented for first time and compared with the results from corresponding non-dispersed bulk phases in excess water. Due to an increased chain conformational order, all inverse self-assemblies swelled with increasing pressure in consistent with previous studies on lyotropic liquid crystalline phases[34, 36, 41], but more interestingly, the lattice parameters for self-assemblies within lipid particles were always greater than the lattice parameters for the bulk self-assemblies at different pressures in the range of 1-1200 bar. Changes in the lattice parameters (Δa in Å) referring to a pressure change (ΔP) of 1000 bar were also higher for phases inside lipid particles as compared to their bulk counterpart. These main findings are explained by both, (i) the possible *influence of the stabilizer F127* on the interfacial curvature and hydration properties, and (ii), by the *differences* in the flexibility and fluctuation motions occurring in dispersed and bulk systems, respectively. In particular, in TC-free samples enhanced bilayer undulations might additionally cause the 'excess water boundary'[66] to shift towards higher solubilized water contents for dispersed cubosome particles. On the other hand, bilayer

undulations in case of bulk TC-free self-assemblies are presumed to be hampered due to rather high viscosity and enclosure by denser lipidic domains in contrast to the assemblies inside lipid particles. Similar arguments are made for the disorder enhancement in particles enveloping discontinuous lipid phases. This notion, however, requires further systematic investigations including careful analysis of disorder difference in bulk and nanoparticulate systems, respectively. Nevertheless, the current work and other studies on barotropic systems are helpful towards understanding the endurance of biomembranes and related organelles of piezophiles under extreme conditions of deep ocean waters. Regeneration of original phases following the compression-decompression steps, and virtual stability of lipid particles validate their robustness for potential rigorous treatments and industrial operations. Such robust nano-carriers could be highly useful for developing a range of biotechnological applications including drugs, peptides, and biomacromolecules delivery.

ACKNOWLEDGMENT

CVK would like to thank Dr. Ulrich Keyser, University of Cambridge for financial support for trip to Elettra, Trieste, Italy.

REFERENCES

1. Luzzati Vittorio; A, T., Lipid phases: structure and structural transitions. *Annu. Rev. Phys. Chem.* **1974,** *25* (79-94).
2. Larsson, K.; Fontell, K.; Krog, N., Structural relationships between lamellar, cubic and hexagonal phases in monoglyceride-water systems. possibility of cubic structures in biological systems. *Chemistry and Physics of Lipids* **1980,** *27* (4), 321-328.
3. Seddon, J. M., Structure of the inverted hexagonal (HII) phase, and non-lamellar phase transitions of lipids. *Biochimica et Biophysica Acta (BBA) - Reviews on Biomembranes* **1990,** *1031* (1), 1-69.
4. Kulkarni, C. V., Lipid crystallization: from self-assembly to hierarchical and biological ordering. *Nanoscale* **2012,** *4* (19), 5779-5791.
5. Kulkarni, C. V.; Wachter, W.; Iglesias, G. R.; Engelskirchen, S.; Ahualli, S., Monoolein: A Magic Lipid? *Phys Chem Chem Phys* **2011,** *13*, 3004-3021.
6. Harper, P. E.; Gruner, S. M., Electron density modeling and reconstruction of infinite periodic minimal surfaces (IPMS) based phases in lipid-water systems. I. Modeling IPMS-based phases. *The European Physical Journal E - Soft Matter* **2000,** *V2* (3), 217-228.
7. Rappolt, M.; Cacho-Nerin, F.; Morello, C.; Yaghmur, A., How the chain configuration governs the packing of inverted micelles in the cubic Fd3m-phase. *Soft Matter* **2013,** *9* (27), 6291-6300.
8. Landau, E. M.; Rosenbusch, J. P., Lipidic cubic phases: A novel concept for the crystallization of membrane proteins. *PNAS* **1996,** *93* (25), 14532-14535.
9. Kulkarni, C. V., *In cubo* crystallization of membrane proteins. In *Advances in Planar Lipid Bilayers and Liposomes*, Iglic, A., Ed. Academic Press: **2010**; Chapter 9, pp 237-272.
10. Wallace, S. J.; Li, J.; Nation, R. L.; Boyd, B. J., Drug release from nanomedicines: Selection of appropriate encapsulation and release methodology. *Drug delivery and translational research* **2012,** *2* (4), 284-292.
11. Angelova, A.; Angelov, B.; Mutafchieva, R.; Lesieur, S.; Couvreur, P., Self-Assembled Multicompartment Liquid Crystalline Lipid Carriers for Protein, Peptide, and Nucleic Acid Drug Delivery. *Accounts of Chemical Research* **2011,** *44* (2), 147-156.
12. Bender, J.; Simonsson, C.; Smedh, M.; Engstrom, S.; Ericson, M. B., Lipid cubic phases in topical drug delivery: visualization of skin distribution using two-photon microscopy. *J Control Release* **2008,** *129* (3), 163-9.
13. Landau, E. M.; Navarro, J. V. Methods and devices for separation of biological molecules. US2001/0025791A1, 4th October, **2001**.
14. Mezzenga, R.; Meyer, C.; Servais, C.; Romoscanu, A. I.; Sagalowicz, L.; Hayward, R. C., Shear Rheology of Lyotropic Liquid Crystals: A Case Study. *Langmuir* **2005,** *21* (8), 3322.
15. Caffrey, M., Membrane protein crystallization. *Journal of Structural Biology* **2003,** *142* (1), 108-132.
16. Gaunt, N. P.; Patil-Sen, Y.; Baker, M. J.; Kulkarni, C. V., Carbon nanotubes for stabilization of nanostructured lipid particles. *Nanoscale* **2015,** *7* (3), 1090-1095.
17. Kulkarni, C. V.; Glatter, O., Hierarchically Organized Systems Based on Liquid Crystalline Phases. In *Self-Assembled Supramolecular Architectures: Lyotropic Liquid Crystals*, Garti, N., Ed. John Wiley & Sons, Inc.: **2012**; Chapter 6.
18. Larsson, K., Colloidal dispersions of ordered lipid-water phases. *Journal of Dispersion Science and Technology* **1999,** *20* (1-2), 27-34.

19. Yaghmur, A.; de Campo, L.; Sagalowicz, L.; Leser, M. E.; Glatter, O., Emulsified Microemulsions and Oil-Containing Liquid Crystalline Phases. *Langmuir* **2005,** *21* (2), 569-577.
20. Clogston, J. Applications of the lipidic cubic phase: From controlled release and uptake to in meso crystallization of membrane proteins. Ohio State Univ., USA., **2005**.
21. Yaghmur, A.; Glatter, O., Characterization and potential applications of nanostructured aqueous dispersions. *Adv Colloid Interface Sci* **2009,** *147-148*, 333-42.
22. Zweytick, D.; Athenstaedt, K.; Daum, G., Intracellular lipid particles of eukaryotic cells. *Biochimica et Biophysica Acta (BBA) - Reviews on Biomembranes* **2000,** *1469* (2), 101-120.
23. Grillitsch, K.; Connerth, M.; Köfeler, H.; Arrey, T. N.; Rietschel, B.; Wagner, B.; Karas, M.; Daum, G., Lipid particles/droplets of the yeast Saccharomyces cerevisiae revisited: Lipidome meets Proteome. *Biochimica et Biophysica Acta* **2011,** *1811* (12), 1165-1176.
24. Fujimoto, T.; Parton, R. G., Not Just Fat: The Structure and Function of the Lipid Droplet. *Cold Spring Harbor Perspectives in Biology* **2011,** *3* (3), a004838.
25. Zehmer, J. K.; Huang, Y.; Peng, G.; Pu, J.; Anderson, R. G. W.; Liu, P., A role for lipid droplets in inter-membrane lipid traffic. *Proteomics* **2009,** *9* (4), 914-921.
26. Phan, S.; Fong, W.-K.; Kirby, N.; Hanley, T.; Boyd, B. J., Evaluating the link between self-assembled mesophase structure and drug release. *International Journal of Pharmaceutics* **2011,** *421* (1), 176-182.
27. Fong, W. K.; Hanley, T.; Boyd, B. J., Stimuli responsive liquid crystals provide 'on-demand' drug delivery in vitro and in vivo. *Journal of Controlled Release* **2009,** *135* (3), 218-226.
28. Rahanyan-Kägi, N.; Aleandri, S.; Speziale, C.; Mezzenga, R.; Landau, E. M., Stimuli-Responsive Lipidic Cubic Phase: Triggered Release and Sequestration of Guest Molecules. *Chemistry – A European Journal* **2014**, n/a-n/a.
29. Paccamiccio, L.; Pisani, M.; Spinozzi, F.; Ferrero, C.; Finet, S.; Mariani, P., Pressure effects on lipidic direct phases: the dodecyl trimethyl ammonium chloride-water system. *The journal of physical chemistry* **2006,** *110* (25), 12410-8.
30. Tyler, A. I. I.; Shearman, G. C.; Brooks, N. J.; Delacroix, H.; Law, R. V.; Templer, R. H.; Ces, O.; Seddon, J. M., Hydrostatic pressure effects on a hydrated lipid inverse micellar Fd3m cubic phase. *Physical Chemistry Chemical Physics* **2011**.
31. Pisani, M.; Bernstorff, S.; Ferrero, C.; Mariani, P., Pressure Induced Cubic-to-Cubic Phase Transition in Monoolein Hydrated System. *The Journal of Physical Chemistry B* **2001,** *105* (15), 3109-3119.
32. Mariani, P.; Paci, B.; Bösecke, P.; Ferrero, C.; Lorenzen, M.; Caciuffo, R., Effects of hydrostatic pressure on the monoolein-water system: An estimate of the energy function of the inverted Ia3d cubic phase. *Physical Review E* **1996,** *54* (5), 5840.
33. Tang, T. Y. D.; Brooks, N. J.; Jeworrek, C.; Ces, O.; Terrill, N. J.; Winter, R.; Templer, R. H.; Seddon, J. M., Hydrostatic Pressure Effects on the Lamellar to Gyroid Cubic Phase Transition of Monolinolein at Limited Hydration. *Langmuir* **2012,** *28* (36), 13018-13024.
34. Brooks, N. J.; Ces, O.; Templer, R. H.; Seddon, J. M., Pressure effects on lipid membrane structure and dynamics. *Chemistry and Physics of Lipids* **2011,** *164* (2), 89-98.
35. Conn, C. E.; Ces, O.; Squires, A. M.; Mulet, X.; Winter, R.; Finet, S. M.; Templer, R. H.; Seddon, J. M., A pressure-jump time-resolved X-ray diffraction study of cubic-cubic transition kinetics in monoolein. *Langmuir* **2008,** *24* (6), 2331-40.
36. Seddon, J.; Squires, A.; Conn, C.; Ces, O.; Heron, A.; Mulet, X.; Shearman, G.; Templer, R., Pressure-jump X-ray studies of liquid crystal transitions in lipids. *Philosophical*

Transactions of the Royal Society A: Mathematical, Physical and Engineering Sciences **2006,** *364* (1847), 2635-2655.
37. Conn, C. E.; Ces, O.; Mulet, X.; Finet, S.; Winter, R.; Seddon John, M.; Templer Richard, H., Dynamics of structural transformations between lamellar and inverse bicontinuous cubic lyotropic phases. *Physical review letters* **2006,** *96* (10), 108-102.
38. Winter, R., Pressure Effects on Artificial and Cellular Membranes. In *High Pressure Bioscience: Basic Concepts, Applications and Frontiers*, Akasaka, K.; Matsuki, H., Eds. Springer: **2015**, p 345.
39. Lai, K.; Wang, B.; Zhang, Y., High Pressure Effect on Phase Transition Behavior of Lipid Bilayers. *Physical Chemistry Chemical Physics* **2012**.
40. Yaghmur, A.; Kriechbaum, M.; Amenitsch, H.; Steinhart, M.; Laggner, P.; Rappolt, M., Effects of pressure and temperature on the self-assembled fully hydrated nanostructures of monoolein-oil systems. *Langmuir* **2010,** *26* (2), 1177-85.
41. Winter, J. E., C Czeslik and A Gabke, Effect of pressure on the stability, phase behaviour and transformation kinetics between structures of lyotropic lipid mesophases and model membrane systems. *J. Phys.: Condens. Matter* **1998.,** *10*, 11499–11518.
42. So, P. T. C.; Gruner, S. M.; Erramilli, S., Pressure-induced topological phase transitions in membranes. *Physical Review Letters* **1993,** *70* (22), 3455.
43. Winter, R.; Jeworrek, C., Effect of pressure on membranes. *Soft Matter* **2009,** *5* (17), 3157-3173.
44. Barriga, H. M. G.; Tyler, A. I. I.; McCarthy, N. L. C.; Parsons, E. S.; Ces, O.; Law, R. V.; Seddon, J. M.; Brooks, N. J., Temperature and pressure tuneable swollen bicontinuous cubic phases approaching nature's length scales. *Soft Matter* **2015,** *11* (3), 600-607.
45. Tang, T. Y. D.; Seddon, A. M.; Jeworrek, C.; Winter, R.; Ces, O.; Seddon, J. M.; Templer, R. H., The effects of pressure and temperature on the energetics and pivotal surface in a monoacylglycerol/water gyroid inverse bicontinuous cubic phase. *Soft Matter* **2014,** *10* (17), 3009-3015.
46. Kraineva, J.; Nicolini, C.; Thiyagarajan, P.; Kondrashkina, E.; Winter, R., Incorporation of [alpha]-chymotrypsin into the 3D channels of bicontinuous cubic lipid mesophases. *Biochimica et Biophysica Acta (BBA) - Proteins & Proteomics* **2006,** *1764* (3), 424-433.
47. Kraineva, J.; Narayanan, R. A.; Kondrashkina, E.; Thiyagarajan, P.; Winter, R., Kinetics of lamellar-to-cubic and intercubic phase transitions of pure and cytochrome c containing monoolein dispersions monitored by time-resolved small-angle X-ray diffraction. *Langmuir* **2005,** *21* (8), 3559-3571.
48. Lendermann, J.; Winter, R., Interaction of cytochrome c with cubic monoolein mesophases at limited hydration conditions: The effects of concentration, temperature and pressure. *Physical Chemistry Chemical Physics* **2003,** *5* (7), 1440-1450.
49. Kulkarni, C. V.; Ces, O.; Templer, R. H.; Seddon, J. M., Pressure effects on a protein-lipid model membrane. *Soft Matter* **2013,** *9* (28), 6525-6531.
50. Qiu, H.; Caffrey, M., The phase diagram of the monoolein/water system: metastability and equilibrium aspects. *Biomaterials* **2000,** *21* (3), 223-234.
51. Guillot, S.; Moitzi, C.; Salentinig, S.; Sagalowicz, L.; Leser, M. E.; Glatter, O., Direct and indirect thermal transitions from hexosomes to emulsified micro-emulsions in oil-loaded monoglyceride-based particles. *Colloids and Surfaces A: Physicochemical and Engineering Aspects* **2006,** *291* (1-3), 78-84.
52. Barauskas, J.; Landh, T., Phase Behavior of the Phytantriol/Water System. *Langmuir* **2003,** *19* (23), 9562-9565.

53. Salonen, A.; Guillot, S.; Glatter, O., Determination of Water Content in Internally Self-Assembled Monoglyceride-Based Dispersions from the Bulk Phase. *Langmuir* **2007,** *23* (18), 9151-9154.
54. Yaghmur, A.; de Campo, L.; Salentinig, S.; Sagalowicz, L.; Leser, M. E.; Glatter, O., Oil-loaded monolinolein-based particles with confined inverse discontinuous cubic structure (Fd3m). *Langmuir* **2006,** *22* (2), 517-21.
55. Amenitsch, H.; Rappolt, M.; Kriechbaum, M.; Mio, H.; Laggner, P.; Bernstorff, S., First performance assessment of the small-angle X-ray scattering beamline at ELETTRA. *J Synchrotron Radiat* **1998,** *5* (Pt 3), 506-8.
56. Steinhart, M.; Kriechbaum, M.; Pressl, K.; Amenitsch, H.; Laggner, P.; Bernstorff, S., High-pressure instrument for small- and wide-angle x-ray scattering. II. Time-resolved experiments. *Review of Scientific Instruments* **1999,** *70* (2), 1540-1545.
57. Duesing, P. M.; Seddon, J. M.; Templer, R. H.; Mannock, D. A., Pressure Effects on Lamellar and Inverse Curved Phases of Fully Hydrated Dialkyl Phosphatidylethanolamines and β-d-Xylopyranosyl-sn-glycerols. *Langmuir* **1997,** *13* (10), 2655-2664.
58. Gustafsson, J.; Ljusberg-Wahren, H.; Almgren, M.; Larsson, K., Submicron Particles of Reversed Lipid Phases in Water Stabilized by a Nonionic Amphiphilic Polymer. *Langmuir* **1997,** *13* (26), 6964-6971.
59. Abraham, T.; Hato, M.; Hirai, M., Glycolipid based cubic nanoparticles: preparation and structural aspects. *Colloids Surf B Biointerfaces* **2004,** *35* (2), 107-17.
60. Hyde, S. T., Bicontinuous structures in lyotropic liquid crystals and crystalline hyperbolic surfaces. *Current Opinion in Solid State and Materials Science* **1996,** *1* (5), 653-662.
61. Muller, F.; Salonen, A.; Glatter, O., Phase behavior of Phytantriol/water bicontinuous cubic Pn3m cubosomes stabilized by Laponite disc-like particles. *Journal of Colloid and Interface Science* **2010,** *342* (2), 392-398.
62. Rizwan, S. B.; Dong, Y. D.; Boyd, B. J.; Rades, T.; Hook, S., Characterisation of bicontinuous cubic liquid crystalline systems of phytantriol and water using cryo field emission scanning electron microscopy (cryo FESEM). *Micron* **2007,** *38* (5), 478-485.
63. Kraineva, J.; Smirnovas, V.; Winter, R., Effects of lipid confinement on insulin stability and amyloid formation. *Langmuir* **2007,** *23* (13), 7118-7126.
64. Dong, Y. D.; Dong, A. W.; Larson, I.; Rappolt, M.; Amenitsch, H.; Hanley, T.; Boyd, B. J., Impurities in commercial phytantriol significantly alter its lyotropic liquid-crystalline phase behavior. *Langmuir* **2008,** *24* (13), 6998-7003.
65. Kulkarni, C. V., Nanostructural studies on monoelaidin-water systems at low temperatures. *Langmuir* **2011,** *27* (19), 11790-800.
66. Katsaras, J., Highly aligned lipid membrane systems in the physiologically relevant "excess water" condition. *Biophysical Journal* **1997,** *73* (6), 2924-2929.
67. Kulkarni, C. V.; Tang, T. Y.; Seddon, A. M.; Seddon, J. M.; Ces, O.; Templer, R. H., Engineering Bicontinuous Cubic Structures at the Nanoscale– the Role of Chain Splay. *Soft Matter* **2010,** *6*, 3191-3194.
68. Briggs, J.; Chung, H.; Caffrey, M., The temperature-composition phase diagram and mesophase structure characterization of the monoolein/water system. *J. Phys. II France* **1996,** *6* (5), 723-751.
69. Landh, T., Phase Behavior in the System Pine Needle Oil Monoglycerides-Poloxamer 407-Water at 20.degree. *The journal of physical chemistry* **1994,** *98* (34), 8453-8467.
70. Yaghmur, A.; Laggner, P.; Almgren, M.; Rappolt, M., Self-assembly in monoelaidin aqueous dispersions: direct vesicles to cubosomes transition. *PLoS One* **2008,** *3* (11), e3747.

71. Gustafsson, J.; Ljusberg-Wahren, H.; Almgren, M.; Larsson, K., Cubic Lipid−Water Phase Dispersed into Submicron Particles. *Langmuir* **1996,** *12* (20), 4611-4613.
72. Carius, W., The compressibility of bimolecular lipid membranes. *Biophys. Struct. Mechanism* **1980,** *6* (1), 90-90.
73. Fine, R. A.; Millero, F. J., Compressibility of water as a function of temperature and pressure. *The Journal of Chemical Physics* **1973,** *59* (10), 5529-5536.
74. Podgornik, R.; Parsegian, V. A., On a Possible Microscopic Mechanism Underlying the Vapor Pressure Paradox. *Biophysical Journal* **1997,** *72* (2 Pt 1), 942-952.
75. Scherrer, P., Bestimmung der Grösse und der inneren Struktur von Kolloidteilchen mittels Röntgensrahlen. *Nachrichten von der Gesellschaft der Wissenschaften zu Göttingen, Mathematisch-Physikalische Klasse* **1918**, 98-100.
76. Pabst, G.; Koschuch, R.; Pozo-Navas, B.; Rappolt, M.; Lohner, K.; Laggner, P., Structural analysis of weakly ordered membrane stacks. *Journal of Applied Crystallography* **2003,** *36* (6), 1378-1388.
77. Shearman, G. C.; Khoo, B. J.; Motherwell, M. L.; Brakke, K. A.; Ces, O.; Conn, C. E.; Seddon, J. M.; Templer, R. H., Calculations of and Evidence for Chain Packing Stress in Inverse Lyotropic Bicontinuous Cubic Phases. *Langmuir* **2007,** *23* (13), 7276-7285.
78. Shearman, G. C.; Ces, O.; Templer, R. H., Towards an understanding of phase transitions between inverse bicontinuous cubic lyotropic liquid crystalline phases. *Soft Matter* **2010,** *6* (2), 256-262.
79. Pabst, G.; Rappolt, M.; Amenitsch, H.; Bernstorff, S.; Laggner, P., X-ray Kinematography of Temperature-Jump Relaxation Probes the Elastic Properties of Fluid Bilayers. *Langmuir* **2000,** *16* (23), 8994-9001.
80. Lide, D. R., *CRC Handbook of Chemistry and Physics, 84th Edition*. Taylor & Francis: **2003**.